Influence of Scaffold Size on Bactericidal Activity of Nitric Oxide-Releasing Silica Nanoparticles

Alexis W. Carpenter, Danielle L. Slomberg, Kavitha S. Rao, and Mark H. Schoenfisch*

Department of Chemistry, University of North Carolina at Chapel Hill, Chapel Hill, North Carolina 27599, United States

ABSTRACT A reverse microemulsion synthesis was used to prepare amine-functionalized silica nanoparticles of three distinct sizes (*i.e.*, 50, 100, and 200 nm) with similar amine content. The resulting hybrid nanoparticles, consisting of *N*-(6-aminohexyl)aminopropyltrimethoxysilane and tetraethoxysilane, were highly monodisperse in size. *N*-Diazeniumdiolate nitric oxide (NO) donors were subsequently formed on secondary amines while controlling reaction conditions to keep the total amount of NO released constant for each particle size. The bactericidal efficacy of the NO-releasing nanoparticles against *Pseudomonas aeruginosa* increased with decreasing particle size. Additionally, smaller diameter nanoparticles were found to associate with the bacteria at a faster rate and to a greater extent than larger particles. Neither control (non-NO-releasing) nor NO-releasing particles exhibited toxicity toward L929 mouse fibroblasts at concentrations above their respective minimum bactericidal concentrations. This study represents the first investigation of the bactericidal efficacy of NO-releasing silica nanoparticles as a function of particle size.

KEYWORDS: nitric oxide · silica nanoparticle · reverse microemulsion · size dependent · bactericidal · antibacterial

The endogenous free radical nitric oxide (NO) is involved in numerous physiological processes, including neurotransmission, wound healing, blood pressure regulation, platelet adhesion, and the immune response.[1−5] While the delivery of exogenous gaseous NO has been shown to elicit promising antimicrobial effects against Gram-positive and Gram-negative bacteria, and even antibiotic-resistant strains,[6] the utility of NO as an effective therapeutic has been limited due to its reactive and concentration-dependent behavior. As a result, much research has focused on the development of NO donors that store and generate NO in a controlled manner.[7−11] Examples of NO donors that reversibly bind NO include metal nitrosyls, *S*-nitrosothiols, *N*-diazeniumdiolates, and organic nitrates. *N*-Diazeniumdiolate NO donors, formed upon the reaction of secondary amines with NO under basic conditions, are of particular interest, as they undergo proton-initiated decomposition in physiological solution (pH 7.4, 37 °C) to release two equivalents of NO per functional group.[7]

Although useful as tools for studying the role of NO in biology, most low molecular weight (LMW) NO donors release NO indiscriminately with undesirable cytotoxicity to healthy cells.[3,12,13] Previously we reported the synthesis of macromolecular NO-releasing silica particles *via* the Stöber method as a new class of NO release materials that store/release substantial levels of NO with great potential for future targeting strategies due to versatile surface chemistries for attaching cell targeting and/or tracking (*i.e.*, fluorescent) ligands.[14,15] Employing a hybrid silica design allowed for a wide range of NO doses and release kinetics by changing the type and concentration of the aminosilane precursor. In a subsequent study,[13] we observed that the silica particles were highly effective at delivering NO to bacteria (*i.e.*, *Pseudomonas aeruginosa*) and were thus significantly more bactericidal than a comparable small molecule NO donor. Our work was corroborated by other recent reports describing the use of nanomaterials to deliver antimicrobial agents.[16] Indeed, nanoparticles composed of silver,[17−20] copper,[21−23] zinc oxide,[24−28] titanium dioxide,[24,29,30] and magnesium oxide exhibit a broad range of bactericidal activity. The bactericidal efficacy of such materials has been proven to be dependent on both the chemical composition and the particle diameter, with smaller diameters generally enhancing killing. Morones *et al.* reported more effective *Escherichia coli* (*E. coli*) killing by smaller diameter (∼1−10 nm) silver nanoparticles due to greater particle interaction with the bacteria.[17] Likewise, Nair *et al.* observed tunable killing as a function of particle size for zinc oxide nanoparticles, with the greatest killing efficacy observed for the smallest particle system prepared.[28] Since particle association with bacteria appears to be critical to antimicrobial activity,[17,31−33] we sought to study the influence of nanoparticle−bacteria interactions and the resulting bactericidal efficacy of NO-releasing

* E-mail: schoenfisch@unc.edu.

Received for review June 3, 2011 and accepted August 15, 2011.

Published online August 15, 2011
10.1021/nn202054f

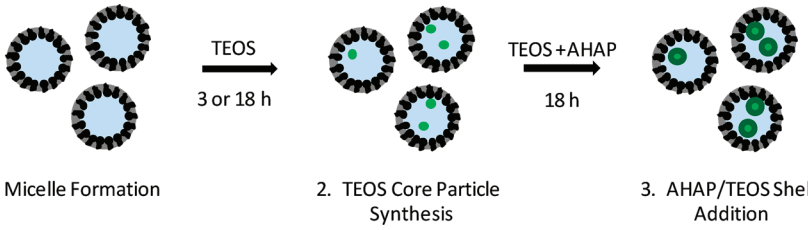

Scheme 1. Synthesis of amine-functionalized silica nanoparticles *via* a reverse microemulsion. Step 1 involves micelle formation. Step 2 is the addition of tetraethoxysilane (TEOS) to the emulsion to form monodisperse "seed" particles. Lastly, step 3 is the subsequent addition of TEOS and AHAP that co-condense to form the AHAP/TEOS silica nanoparticles.

nanoparticles. Herein, we describe the reverse microemulsion synthesis of monodisperse NO-releasing silica particles of three distinct sizes (50, 100, and 200 nm) with equal NO release and the evaluation of their size-dependent antibacterial action against *Pseudomonas aeruginosa*.

RESULTS AND DISCUSSION

While metallic and metal oxide nanoparticles with diameters of 1 to 500 nm have been reported to exhibit toxicity toward both Gram-positive and Gram-negative microorganisms, nanoparticles of diameters $\leq$100 nm are generally more effective biocides.[16] As such, we set out to investigate the influence of particle size on the bacteria killing efficacy of NO-releasing silica particles with diameters above, below, and equal to 100 nm. To achieve these specific sizes, the reverse microemulsion technique was used, as it provides a method for synthesizing silica-based particles in the nanometer range with excellent control over size and particle composition by changing any number of synthetic parameters, including the amount of water and ammonium hydroxide,[34−36] reaction time, the type of organic solvent, and the ratios of water to surfactant, surfactant to co-surfactant, and surfactant to organic solvent.[36−38] A clear benefit of this method is the ability to tune particle size while keeping the aminoalkoxysilane:alkoxysilane ratio constant.[34,39−41] In general, particles synthesized by the reverse microemulsion method have a smaller size and narrower distribution than those produced *via* the Stöber method.[37,42] Narrow size distributions are essential when investigating the influence of nanoparticle size on bacterial interactions. Furthermore, the use of the reverse microemulsion technique provides a facile method for core−shell particle designs such that a variety of functionalities are easily incorporated as part of the silica scaffold.[34,37,39−41,43]

Size-Controlled Synthesis of Amine-Functionalized Silica Nanoparticles. Scheme 1 illustrates the reverse microemulsion approach used to obtain amine-functionalized silica nanoparticles. For the three sizes (50, 100, and 200 nm), the micelles were prepared using Triton X-100 (surfactant) and 1-hexanol (co-surfactant) suspended in pentane or heptane. Following micelle formation, an aqueous phase was introduced by adding water and ammonium hydroxide, sequentially. Following the formation of a stable microemulsion as indicated by a clear and colorless solution (step 1 of Scheme 1), the amine-modified silica nanoparticles were synthesized. *N*-(6-Aminohexyl)aminopropyltrimethoxysilane (AHAP) and tetraethoxysilane (TEOS) were chosen for study on the basis of prior work that demonstrated NO-releasing AHAP/TEOS particles to be effective against *P. aeruginosa* and not toxic to fibroblast cells.[13] The addition of pure aminosilane to the microemulsion resulted in amorphous silica particulates at low yields (1−2 mg). Thus, it was necessary to include a tetraalkoxysilane backbone to promote condensation as was seen for our previously reported particle systems.[14,15] However, the simultaneous addition of both AHAP and TEOS resulted in particles of a wide size distribution, especially at high AHAP concentrations. By adopting a sequential silane addition method, the monodispersity of the particles was greatly improved. Thus, TEOS was added initially to the microemulsion to form monodisperse TEOS seed particles (step 2 of Scheme 1) prior to shell modification with 65 mol % AHAP (balance TEOS), as shown in step 3 of Scheme 1. The reverse microemulsion process allowed for higher aminosilane incorporation than was previously achievable *via* the Stöber process (10 mol %, balance TEOS)[14] due to diffusion-controlled particle growth. Of note, adding AHAP alone to the microemulsion resulted in poor shell formation and low yield. Due to the mismatched hydrolysis and condensation rates of the two silane precursors,[44] TEOS was added 30 min prior to the addition of AHAP during shell modification to achieve monodisperse particle populations.

To tune particle size, a variety of synthetic parameters were adjusted (Table 1). The viscosity, polarity, and

TABLE 1. Variable Synthetic Parameters for Each Amine-Functionalized Nanoparticle Size

	organic solvent		
particle size (nm)	type	volume (mL)	TEOS core particle reaction time (h)
50	pentane	45.6	3
100	heptane	15.2	3
200	heptane	15.2	18

TABLE 2. Particle Size As Determined by Transmission Electron Microscopy (TEM) and Dynamic Light Scattering (DLS) and Zeta Potential as Determined by Laser Doppler Velocimetry

	TEM	DLS[a]				zeta potential[b]	
particle size (nm)	diameter (nm)	Z-Ave (nm)	PDI	number PSD (nm)	volume PSD (nm)	R_2NH (mV)	$R_2N[N(O)NO]^-$ (mV)
50	56 ± 7	80.0 ± 3.1	0.150 ± 0.041	52.7 ± 3.3	66.8 ± 3.4	+11.8 ± 1.2	−5.2 ± 3.9
100	93 ± 14	129.5 ± 13.7	0.087 ± 0.042	98.4 ± 6.7	127.3 ± 11.9	+12.5 ± 1.1	+5.9 ± 2.3
200	199 ± 27	209.0 ± 3.9	0.041 ± 0.029	191.0 ± 1.8	221.7 ± 8.8	+11.4 ± 1.1	+8.4 ± 0.3

[a] In phosphate-buffered saline (pH 7.4) at 37 °C. [b] In phosphate buffer (pH 7.4) at 37 °C.

molecular structure of the organic solvent are known to influence the intermolecular forces between the surfactant molecules and the organic phase, and thus greatly impact the micelle diameter and the resulting particle size.[45] Smaller organic solvent molecules can penetrate deeper into the surfactant layer, decreasing the overall size of the water droplet and ensuing particles.[37] For this reason, pentane was used to prepare the smallest AHAP/TEOS particles (*i.e.*, 50 nm), while heptane was used to form the larger diameter particles (*i.e.*, 100 and 200 nm). Additionally, increasing the volume of organic solvent decreases the occurrence of interdroplet percolation, resulting in smaller particles. Decreasing reaction time can also ultimately lead to smaller particles.[37] For example, a 3 h TEOS seed reaction resulted in 5 nm particles, whereas 12 nm seed particles were achieved after 18 h under the same solvent conditions.

The resulting particle sizes and surface charges of the three synthesized systems are provided in Table 2. While electron microscopy provided a means to examine particle morphology, dynamic light scattering (DLS) allowed for the measurement of the hydrodynamic diameter and solution behavior of the particles.[46] When interpreting nanoparticle size, both DLS and electron microscopy data must be considered together for proper size characterization, as particle size measurements from DLS better represent the entire particle population and the actual size in solution. The Z-average (Z-ave) diameter, polydispersity index (PDI), particle size distributions (PSD), and diameter as measured from transmission electron microscopy (TEM) are provided in Table 2. Taken together, the parameters reported in Table 2 provide a comprehensive evaluation of the actual particle sizes present during bacteria assays. Although no official standard exists, a PDI of <0.2 is considered to be monodisperse, while a PDI of ≤0.1 is considered to be highly monodisperse.[47] With respect to the synthesized silica particles, we observed increasing PDI values as the particle diameter decreased, indicating that while all sizes were monodisperse and formed stable suspensions in phosphate-buffered saline (PBS), decreasing particle size resulted in a slight increase in size distribution. This monodispersity was further corroborated by TEM (Table 2; Supporting Information). Collectively, the DLS and TEM data indicate

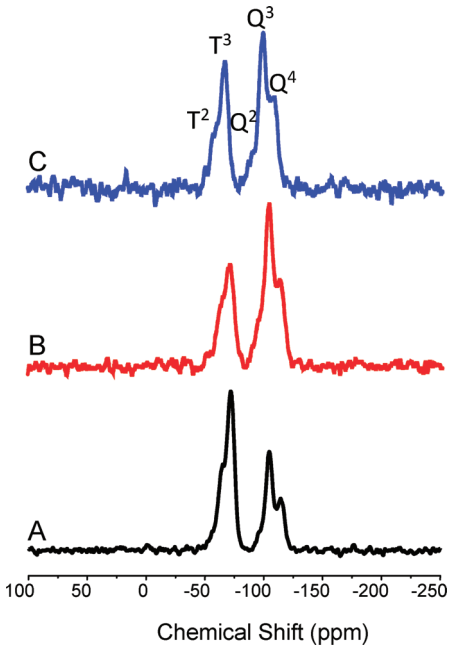

Figure 1. Solid-state CP/MAS ^{29}Si NMR of (A) 50 nm, (B) 100 nm, and (C) 200 nm AHAP/TEOS nanoparticles. The T-band (ca. −70 ppm) represents silicon atoms that are bound to three oxygen atoms (*i.e.*, AHAP). The Q-band (ca. −100 ppm) indicates silicon atoms with four siloxane bonds (*i.e.*, TEOS).

that these particle systems are suitable for investigating the influence of particle size on particle−bacteria interactions based on their narrow size distribution and solution stability.

Solid-state ^{29}Si nuclear magnetic resonance (NMR) confirmed the covalent incorporation of the aminosilane into the silica network. Cross-polarization (CP) and magic angle spinning (MAS) techniques were used to enhance the sensitivity toward silicon atoms near CH_x or OH groups and improve peak resolution.[48,49] As shown in Figure 1, the spectrum of each particle system contained both T- and Q-bands, representing silicon atoms that are bound to three (AHAP) and four (TEOS) oxygen atoms, respectively. Changes in the neighboring oxygen environments surrounding the observed silicon atom were indicated by peak splitting within the T- and Q-bands denoted by superscripted numbers corresponding to the number of siloxane bonds.[48] The ^{29}Si NMR spectra therefore confirmed successful co-condensation and

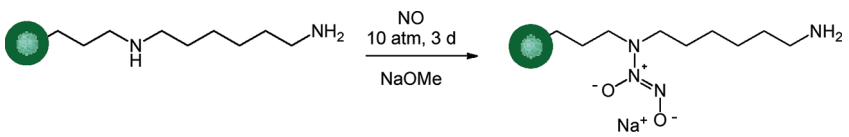

Scheme 2. *N*-Diazeniumdiolate formation on amine-functionalized silica nanoparticle.

TABLE 3. Nitrogen Content, NO Release Properties, and Extent of Amine to *N*-Diazeniumdiolate Conversion for the Amine-Functionalized Silica Nanoparticles

		$[NO]_t$[b] (μmol mg^{-1})					
particle size (nm)	μmol of AHAP[a] per mg particle	2 h	total	% conversion[c]	$[NO]_m$[d] (ppm mg^{-1})	t_m[e] (min)	t_d[f] (h)
50	1.93	0.47 ± 0.02	1.49 ± 0.29	39	49.7 ± 16.8	0.8 ± 0.1	15.2 ± 2.1
100	2.37	0.38 ± 0.01	1.26 ± 0.17	27	43.5 ± 5.2	0.6 ± 0.1	13.0 ± 3.8
200	1.89	0.42 ± 0.01	1.01 ± 0.08	27	44.7 ± 8.0	0.7 ± 0.1	9.9 ± 1.6

[a] Determined by CHN elemental analysis of control particles. [b] $[NO]_t$, total number of moles of NO released per mg of particle as measured by the Griess assay. [c] Based on the assumption that 100% diazeniumdiolate conversion would result in 2 mol of NO per 1 mol of AHAP in particle scaffold. [d] $[NO]_m$, maximum instantaneous concentration of NO released as measured with NOA. [e] t_m, time required to reach $[NO]_m$. [f] t_d, duration of NO release.

incorporation of AHAP and TEOS into the scaffold for each particle size. Of note, the ratios of the T-band to Q-band intensities are not reflective of the actual ratios of AHAP to TEOS within the particle because the core particles are likely pure SiO_2 and free of hydrogens.

Elemental analysis allowed for a more quantitative investigation of AHAP concentration within each particle system. We hypothesized that the amine content would remain constant regardless of particle diameter because the molar amounts of silane precursors (both TEOS and AHAP) were held constant for all three systems. The wt % N measured from CHN analysis may be translated to AHAP concentration, as it is the only nitrogen-contributing component within the silica network. For the smallest particle system (50 nm), we measured a wt % N of 5.39, corresponding to 1.93 μmol AHAP per mg of particles. While the nitrogen amount increased slightly for the 100 nm particles (6.64 wt % N or 2.37 μmol AHAP per mg of particles), the larger, 200 nm particle system was characterized by a slightly lower nitrogen content (5.29 wt % N corresponding to 1.89 μmol N per mg of particles), indicating a similar amine content regardless of a change in particle size for the three systems synthesized here.

***N*-Diazeniumdiolate NO Donor Functionalization.** Nitric oxide was loaded onto the silica scaffolds *via* *N*-diazeniumdiolate formation on the secondary amine sites of AHAP by exposing the particles to a high pressure of NO in the presence of a base catalyst (NaOMe) (Scheme 2).[14,50] *N*-Diazeniumdiolate formation was confirmed *via* NO release and zeta potential (*i.e.*, surface charge) changes observed after NO loading (Table 2). Initially, each particle system was characterized by a slightly positive charge of ca. +12 mV, an expected result due to the protonated primary amines at pH 7.4. Following NO loading, the zeta potential for each size became neutral (zeta potential between −10 and +10 mV)[51] due to the contribution of the zwitterionic *N*-diazeniumdiolate functionality (Scheme 2). The particles regained their positive charge within 10 min as the result of *N*-diazeniumdiolate decomposition and regeneration of parent amines.

As shown in Table 3, the total amount of NO released from the particles was 1.49 ± 0.29, 1.26 ± 0.17, and 1.01 ± 0.08 μmol mg^{-1} for the 50, 100, and 200 nm AHAP/TEOS particles, respectively. On the basis of the AHAP content per mg particle (Table 3), NO donor loading efficiencies were determined to be 39%, 27%, and 27% for 50, 100, and 200 nm particles, respectively. Such NO loading efficiency is consistent with previously reported *N*-diazeniumdiolate-modified silica particles.[14,50] The greater conversion efficiency for the smallest particle size may be attributed to the increased surface area to volume ratio, resulting in a larger concentration of amines nearer to the particle surface and therefore more accessible to reaction. These hybrid silica particles had very low porosity with surface areas (S_{BET}) of 4−20 m^2/g and pore volumes of 0.008−0.989 cm^3/g (at p/p_o = 0.99), as determined from nitrogen adsorption−desorption isotherms. Indeed, the high density and low porosity resulting from the co-condensation method used to synthesize amine-modified hybrid silica materials have been previously observed.[14,15] As a result of low porosity, amine sites farther from the particle surface are less accessible to diazeniumdiolation. To ascertain the dose of NO delivered from the particles over the course of the bactericidal assays, the total amounts of NO released over 2 and 24 h were measured and are provided in Table 3. As expected, each particle system was depleted of NO by 24 h. The NO release data indicates that over the course of 24 h bacteria were exposed to similar amounts of NO regardless of nanoparticle size, as there is no statistical difference in the total amount of NO released from each particle system. Since NO release occurs

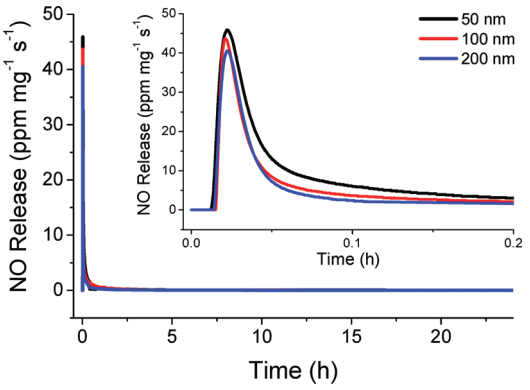

Figure 2. Real-time NO release profile for 50 (black), 100 (red), and 200 (blue) nm NO-releasing AHAP/TEOS particles from $t = 0$ to $t = 24$ h. Inset: NO release from $t = 0$ to $t = 0.2$ h, corresponding to the shortest time period at which particle–bacteria association was investigated with confocal microscopy.

upon protonation of the secondary amine of the *N*-diazeniumdiolate, it is inevitable that the kinetics of NO release differ slightly for each particle size based on the *N*-diazeniumdiolate groups' proximity to the particle surface and therefore differing rate of contact with the aqueous solvent. As shown in Figure 2, the instantaneous release of NO from the particles was characterized by an initial burst of NO due to immediate decomposition of surface *N*-diazeniumdiolate NO donors upon solution immersion. This instantaneous maximum concentration of NO release is defined as $[NO]_m$. The particles exhibited a $[NO]_m$ of 49.7, 43.5, and 44.7 ppm mg^{-1} from the 50, 100, and 200 nm particles, respectively.

Effect of Nanoparticle Size on Bactericidal Activity against *Pseudomonas aeruginosa*. Based on prior work suggesting particles less than 100 nm are more effective antimicrobial materials,[16] we hypothesized that the 50 nm NO-releasing silica nanoparticles would be more effective at bacteria killing than the larger 100 and 200 nm particles. Minimum bactericidal concentration (MBC) assays were performed under nutrient-free conditions in phosphate-buffered saline (PBS) to eliminate bacteria replication, as our goal was to more accurately emphasize the role of size on the particle's bactericidal activity. The MBC was determined as a function of NO-releasing nanoparticle size against 10^6 colony forming units (cfu) mL^{-1} *P. aeruginosa* cultures. The minimum particle concentrations required to achieve complete killing (3 log reduction) after short (2 h) and long (24 h) exposures were thus determined using bacteria in the healthiest state (*i.e.*, mid-log growth stage).[52] After 2 h, the smaller particles were notably more effective at killing *P. aeruginosa* compared to larger particles ($MBC_{2\,h}$ of 0.8 mg mL^{-1} for 50 nm *versus* 1.5 mg mL^{-1} for 100 and 200 nm NO-releasing AHAP/TEOS particles, respectively). This 2-fold difference in $MBC_{2\,h}$ is significant given that there is only a slight difference in total NO released after 2 h from each particle size (Table 3). The total NO released from each particle size after 24 h was not statistically different, yet a 2-fold difference in $MBC_{24\,h}$ was still observed. Furthermore, the increased NO release exposure resulted in nearly a 4-fold decrease in the particle concentrations required to kill *P. aeruginosa* with $MBC_{24\,h}$ of 0.2 mg mL^{-1} for 50 and 100 nm and 0.4 mg mL^{-1} for 200 nm NO-releasing particles. Of note, the 100 nm particles exhibited similar bactericidal properties to the 200 nm particles at short incubation times, while at longer periods the bactericidal efficacy of the 100 nm particles resembled that of the 50 nm nanoparticles. These data corroborate the well-known relationship between biocidal activity and materials on the nanoscale (*i.e.*, materials with size measuring 100 nm or less in one dimension). The considerable decrease in MBC over time indicates that the efficacy of the NO-releasing nanoparticles improves as more NO is released. Neither blanks (*i.e.*, in PBS only) nor control (non-NO-releasing) AHAP/TEOS particles at MBC concentrations affected *P. aeruginosa* viability (Supporting Information).

Although the observed relationship between particle size and MBC may be expected, the mechanism for this phenomenon remained uncertain. Confocal microscopy was thus used to qualitatively observe particle fate. To allow for visualization using fluorescence imaging, the surface-accessible primary amines of the AHAP particles were chemically modified with rhodamine isothiocyanate (RITC).[53] Although NO release was decreased slightly (by 9%), no change in particle size or particle surface charge was observed following RITC modification. Similar to the non-fluorescent particles, a slight decrease in zeta potential was noted following diazeniumdiolation of the RITC-modified particles (ca. +13 mV to ca. +7 mV for control and NO-releasing, respectively). Initially, a time-based experiment was conducted where the bacteria were treated with RITC-modified NO-releasing AHAP/TEOS particles, and images were collected at 20 s intervals over the course of 40 min. The particles rapidly associated with the bacteria within 2 min (Supporting Information), a favorable attribute given the bolus release of NO. Immediately following this interaction, membrane degradation, cellular collapse, blebbing and decreased bacterial adhesion to the substrate were observed and attributed to the antimicrobial action of NO (*e.g.*, lipid peroxidation) (Supporting Information).[54] Such severe morphological changes hindered our ability to distinguish between individual bacteria cells. Thus, the remaining confocal experiments were carried out using RITC-modified control AHAP/TEOS particles to maintain bacteria viability and potentially glean information on particle–bacteria association. Given that the size and surface charge are similar between the NO-releasing and control RITC-modified particles, particle–bacteria interactions that occur with control

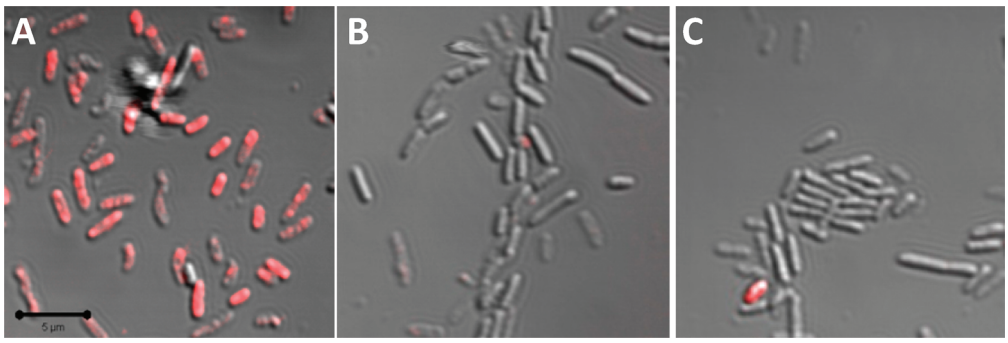

Figure 3. Overlay of fluorescence and bright-field scanning confocal microscopy images of *P. aeruginosa* treated with 10 μg mL^{-1} of (A) 50, (B) 100, and (C) 200 nm RITC-modified AHAP/TEOS silica nanoparticles for 10 min. Magnification is 63×, and scale bar is 5 μm.

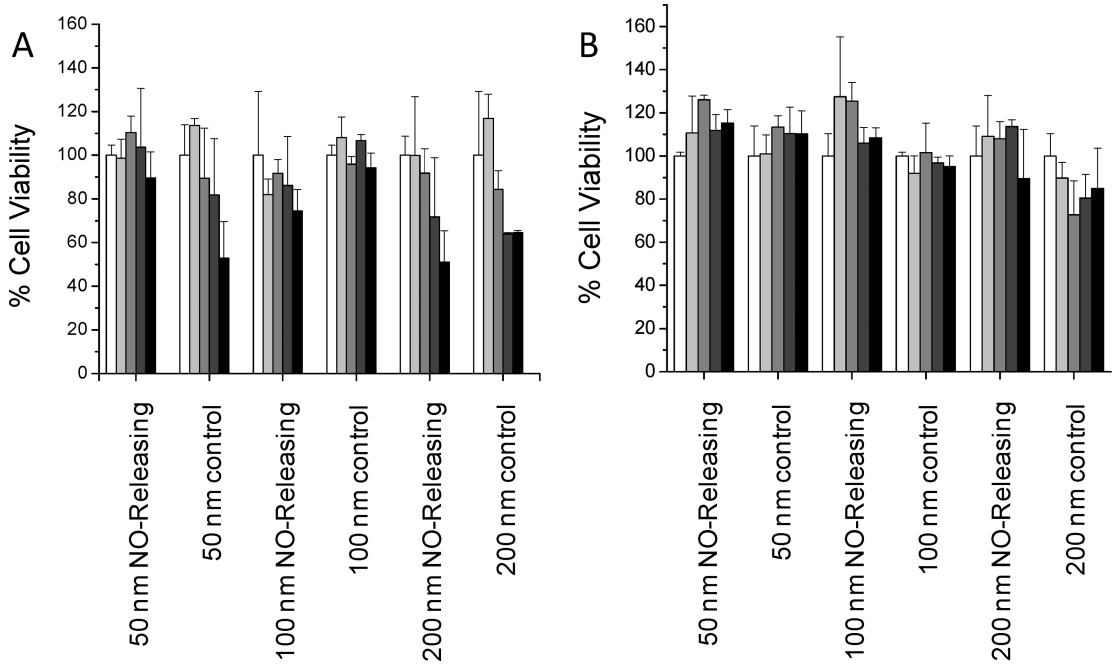

Figure 4. Cytotoxicity of control and NO-releasing particles against L929 mouse fibroblast cells as measured using the MTS assay after (A) 2 h exposure at 0 (white), 0.4 (light gray), 0.8 (gray), 1.6 (dark gray), and 3.2 (black) mg mL^{-1} and after (B) 24 h exposure at 0 (white), 0.1 (light gray), 0.2 (gray), 0.4 (dark gray), and 0.8 (black) mg mL^{-1}.

particles are an accurate representation of those that occur with NO-releasing RITC particles. When *P. aeruginosa* were exposed to particles at 50 μg mL^{-1} for longer than 30 min, fluorescence was present in all bacteria regardless of the particle size. By exposing the bacteria to decreased doses of 50, 100, and 200 nm RITC-modified nanoparticles (*i.e.*, 10 μg mL^{-1}) for shorter time (*i.e.*, 10 min), a difference in the rate and extent of association was observed fluorescently (Figure 3). The greatest RITC fluorescence was observed upon treatment of bacteria with the 50 nm nanoparticles (Figure 3A). Bacteria exposed to 100 nm nanoparticles exhibited some fluorescence but at a lower magnitude than the 50 nm treated cells (Figure 3B). Finally, little fluorescence was observed from the cells treated with the 200 nm particles (Figure 3C). Collectively, these results indicate that although all particle systems tested interact with the bacteria, the smaller diameter particles do so more rapidly. As shown in the inset of Figure 2 and provided in Table 3, a large amount of NO is released within the initial 10 min. Therefore, the rate of association governs the amount of NO delivered directly to the bacteria. Greater association with decreasing particle diameter corroborates our finding that smaller particles were more bactericidal at lower concentrations than larger particles. Indeed, the faster diffusion rate of smaller particles allows for a more rapid association with bacteria. As such, a larger portion of the stored NO is likely delivered to the bacteria from the 50 nm particles compared to the 100 and 200 nm particles, thereby lowering the necessary particle dose and overall NO concentrations required for effective killing.

Cytotoxicity against L929 Mouse Fibroblasts. The use of NO-donor-functionalized silica scaffolds is motivated by both the synthetic versatility and biologically inert qualities of silica.[55] To be useful as a potential therapeutic, such materials must possess favorable toxicity to normal cells. The cytotoxicity of both NO-releasing and control AHAP/TEOS particles was thus evaluated against L929 mouse fibroblasts. Fibroblast viability screening represents a first test for evaluating cytotoxicity of both systemic and topical antibacterial agents, as these cells play a critical role in wound healing.[56,57] Although our lab has previously observed that AHAP/TEOS particles synthesized *via* the Stöber method exhibited no toxicity toward fibroblast cells,[13] the cytotoxicity of the particles reported herein was not obvious due to the modified synthesis (*i.e.*, reverse microemulsion). In addition, our prior report did not investigate the role of size on toxicity. The MTS assay was used to measure cell viability after exposure to both control and NO-releasing particles for 2 and 24 h to mimic the two exposure times of the bactericidal assays. Particle concentrations up to double the MBC values for each time point were tested to evaluate cytotoxicity above the concentration required for bacteria killing. Theoretical total NO doses delivered from each particle concentration after 2 and 24 h were calculated from the NO release data (Table 3) and are provided in Supporting Information. As shown in Figure 4A, no toxicity was observed after 2 h from the NO-releasing particles up to their respective $MBC_{2\,h}$ doses regardless of particle size. Control particles of 50 and 100 nm were also not toxic at their respective bactericidal concentrations. However, the $MBC_{2\,h}$ dose of control 200 nm particles (1.6 mg mL^{-1}) decreased fibroblast viability by 36%. Although toxicity was observed at the highest concentration tested (3.2 mg mL^{-1}) for control 50 nm and both NO-releasing and control 200 nm particles, we note that these concentrations were well above the therapeutic doses required for complete bacteria killing (0.8 and 1.5 mg mL^{-1}, respectively). As shown in Figure 4B for 24 h treatment, no significant toxicity was observed for either NO-releasing or control particles at concentrations up to 2 $\times$ $MBC_{24\,h}$ for all three sizes. Taken together, these results indicate that increased treatment time with NO-releasing AHAP/TEOS particles has the combined advantage of lower therapeutic dose required for sufficient bacteria killing with negligible effect on fibroblast cell viability.

CONCLUSION

A reverse microemulsion synthesis was developed to prepare three sizes of highly monodisperse amine-functionalized silica nanoparticles. The particles were characterized by high amine loading with surface-accessible primary amines that allowed for straightforward coupling of fluorescent markers. Conjugation of other biorecognition agents should be compatible in the same way, further expanding the potential therapeutic utility of these scaffolds. By maintaining constant NO loading/release for each particle size, the relationship between nanoparticle size and bactericidal efficacy was probed. At shorter exposure time, the smaller NO-releasing silica nanoparticles (50 nm) were found to exhibit the greatest bactericidal activity. Such behavior may be attributed to their increased rate of association and subsequent greater NO payload delivered directly to the bacteria. We hypothesize that increasing the rate at which NO-releasing particles associate with bacteria may further improve their antibacterial properties. Future research should focus on how the amount and kinetics of NO delivered to bacterial cells influences the observed bactericidal efficacy. Although particles with both neutral and positive surface charges were shown to interact with the bacteria, the rate of particle association is likely influenced by particle surface charge as bacteria are characterized by a net negative charge. More effective antibacterial nanoparticle therapeutics may be realized by understanding the role of particle−bacteria interactions on bactericidal activity.

EXPERIMENTAL SECTION

Materials. Tetraethoxysilane (TEOS) and *N*-(6-aminohexyl)-aminopropyltrimethoxysilane (AHAP) were purchased from Gelest (Morrisville, PA). Triton X-100, 1-hexanol, heptane, pentane, sodium methoxide (NaOMe, 5.4 M solution in methanol), *N*,*N*-dimethylformamide (DMF), methanol, and rhodamine isothiocyanate were purchased from Acros Organics (Morris Plains, NJ). Ethanol, butanol, and 1-propanol were purchased from Fisher Scientific (Fair Lawn, NJ). Tryptic soy broth, tryptic soy agar, and minimum essential media (MEM) were purchased from Becton, Dickinson and Company (Sparks, MD). *Pseudomonas aeruginosa* (ATCC #19143) was purchased from American Type Culture Collection (Manasses, VA). L929 mouse fibroblasts were obtained from the UNC Tissue Culture Facility (Chapel Hill, NC). Nitric oxide (99.5%), nitrogen (N_2), and argon (Ar) gases were purchased from National Welders (Raleigh, NC). Distilled water was purified using a Millipore Milli-Q UV Gradient A-10 system (Bedford, MA), resulting in a total organic content of $\leq$6 ppb and a final resistivity of 18.2 m$\Omega\cdot$cm.

Reverse Microemulsion Synthesis of Amine-Functionalized Silica Nanoparticles. Amine-functionalized silica nanoparticles of select sizes were synthesized by adjusting the type and volume of organic solvent used in the reverse microemulsion.[37,40,43] Initially, reverse micelles were formed by mixing 3.54 g of Triton X-100, 3.6 mL of 1-hexanol, and the appropriate amount and type of organic solvent for 30 min. Then, 240 μL of water, 120 μL of ammonium hydroxide solution (28 wt % in water), and 40 μL of TEOS were added sequentially in 30 min intervals. Hydrolysis and condensation were allowed to proceed for 3 or 18 h, depending on the desired particle size, to form a TEOS

seed particle. The organic solvent type and volume as well as the reaction time for initial TEOS seed growth for each particle size are listed in Table 1. Following the formation of the TEOS core particle, an additional 40 μL (0.179 mmol) of TEOS was added to the microemulsion, after which 84 μL (0.335 mmol) of AHAP was added 30 min later. Hydrolysis and co-condensation of TEOS and AHAP were allowed to proceed for an additional 18 h to form the amine-functionalized shell. The emulsion was broken upon the addition of ethanol. Silica precipitates were collected *via* centrifugation at 3645*g* for 5 min. The supernatant was removed, and the particles were washed by resuspension in 1-butanol, 2-propanol, and ethanol, sequentially. To ensure removal of Triton X-100, particles were resuspended in 45 mL of a 50/50 ethanol/water (v/v) solution, sonicated for 5 min in chilled water, and collected *via* centrifugation (3645*g*, 5 min). This process was repeated three times before a final wash with ethanol to aid in drying of the particles. The resulting surfactant-free particles (confirmed by UV−vis) were dried *in vacuo* overnight. Product yields were typically between 10 and 20 mg per reaction.

***N*-Diazeniumdiolation of Amine-Functionalized Silica Nanoparticles.** The procedure for loading NO onto the core−shell particles was modified from a previously reported method.[14,50] Briefly, particles were suspended in a 1:9 mixture of DMF and methanol (5 mg mL^{-1}) by sonication. Sodium methoxide, the base catalyst (5.4 M in MeOH), was added in either a 2.5:1 for 50 nm particles or 5:1 for 100 and 200 nm particles molar ratio relative to the concentration of secondary amines as determined by elemental analysis. Following thorough mixing of this solution (vortexed for 1 min), 3.5 mL aliquots were placed in vials equipped with a stir bar. The open vials were then placed in a 160 mL Parr general purpose stainless steel pressure vessel with magnetic stirring and connected to an in-house NO reactor. Oxygen was removed from the solutions by purging with Ar three times rapidly, followed by three 10 min Ar purges at 8 bar. The vessel was then filled to a pressure of 10 bar with NO that had been scrubbed with KOH. The pressure in the reactor was maintained at 10 bar for 72 h by repressuring with fresh NO to accommodate loss due to reaction and/or gas leak. After 72 h, the NO was released from the vessel, and the solutions were again purged with Ar to remove unreacted NO. The resulting *N*-diazeniumdiolate-modified silica nanoparticles were collected by centrifugation (3645*g*, 5 min), washed three times with ethanol, and dried *in vacuo*. The NO donor-modified nanoparticles were then stored in a vacuum-sealed package at −20 °C until further use (up to one week). No loss in NO loading was observed for particles stored in this manner up to 8 d (the longest period investigated) as determined by chemiluminescence upon comparing NO release immediately following diazeniumdiolate formation to that measured on day 8.

Nitric Oxide Release Measurements. Total amounts of NO released from each particle size were evaluated using the Griess assay.[58] The NO-loaded particles were placed in oxygenated PBS, upon which the liberated NO is oxidized to nitrite (NO_2^-). After removing the particles via centrifugation, the supernatant containing NO_2^- was reacted with 1 wt % solutions of sulfanilamide and *N*-1-naphthylethylenediamine to form an azo compound. By detecting the absorbance at 540 nm and comparing the results to a calibration curve, the concentration of NO released from the particles is deduced. While the Griess assay allows for the measurement of total NO concentrations, real-time diazeniumdiolate degradation and NO release kinetics were determined using a Sievers NOA 280i chemiluminescence NO analyzer (Boulder, CO) in PBS (pH 7.4) at 37 °C, as described previously.[59] The absence of nitrite byproducts was confirmed by equal total NO concentrations measured from the Griess assay and the NOA. Prior to analysis, the NO analyzer was calibrated with air passed through a NO zero filter (0 ppm NO) and a 26.39 ppm NO standard gas (balance N_2).

Nanoparticle Characterization. The hydrodynamic particle diameter and zeta potential (*i.e.*, surface charge) were measured using a Malvern Zetasizer Nano-ZS (Malvern Instruments, Ltd.; Worcestershire, UK) equipped with a 10 mW HeNe laser (633 nm) and a NIBS detector at an angle of 173°. All samples were prepared at 1 mg/mL concentrations in PBS (size) or phosphate buffer (zeta potential) and analyzed at 37 °C to mimic the media used for NO-release and bacteria assays. Phosphate buffer (nonsaline, pH 7.4) was employed for zeta potential measurements because the high ionic content of PBS was found to corrode the folded capillary electrodes.[51] Particle size and morphology were also characterized using a JEOL 100 CX II transmission electron microscope at 100 kV.

Covalent incorporation of AHAP and TEOS within the silica network was confirmed using solid-state cross-polarization/magic angle spinning (CP/MAS) ^{29}Si NMR with a Bruker 360 MHz DMX spectrometer (Billerica, MA) equipped with wide-bore magnets (triple-axis pulsed field gradient double-resonance probes). Samples were packed into a 4 mm rotor (double-resonance frequency of 71.548 Hz) and spun at a speed of 10 kHz. Chemical shifts were determined in parts per million relative to a tetramethylsilane external standard. Elemental analysis was performed using a PerkinElmer CHN/S O elemental analyzer Series 2400 (Waltham, MA) instrument.

Bactericidal Assays. *P. aeruginosa* was cultured to a concentration of 10^8 colony forming units (cfu) per mL, collected *via* centrifugation, resuspended in sterile PBS, and adjusted to a concentration of 10^6 cfu mL^{-1}. This starting concentration was chosen to accurately show at least 3 logs reduction, as the limit of detection for the plate-counting method is 2.5×10^3 cfu mL^{-1}.[52] Aliquots of the 10^6 cfu mL^{-1} bacteria suspension were added to pre-massed amounts of nanoparticles to obtain the following concentrations: 0, 0.025, 0.05, 0.1, 0.2, 0.3, 0.4, 0.5, 0.6, 0.7, 0.8, 0.9, 1.0, 1.1, 1.2, 1.3, 1.4, 1.5, and 1.6 mg mL^{-1}. The nanoparticle/bacteria suspensions were vortexed for 30 s to adequately suspend the nanoparticles, then incubated at 37 °C with gentle agitation. Aliquots were then taken from each suspension after 2 and 24 h and diluted 10- and 100-fold in PBS before plating on tryptic soy agar. Bacterial viability was measured after incubating plates at 37 °C overnight by counting observed colonies.

Confocal Microscopy Studies. Nanoparticles were fluorescently labeled by covalent modification with rhodamine isothiocyanate.[53] Briefly, 50 mg of particles were suspended in 100 mL of ethanol and mixed with 5 mg of RITC, protected from light, for 48 h. The particles were then washed copiously with ethanol using the suspension/centrifugation method described above until a colorless supernatant was achieved. All confocal images were obtained with a Zeiss 510 Meta laser scanning confocal microscope. Bright-field and fluorescent images (543 nm HeNe excitation laser) were collected at room temperature with a N.A. 1.2 C-apochromat water immersion lens with either a 40× or 63× objective as indicated for each image. *P. aeruginosa* cultures (10^6 cfu mL^{-1}) were placed in a glass bottom Petri dish and allowed to adhere for 45 min at 37 °C prior to imaging. The slide was then rinsed with fresh PBS to remove loosely or unadhered bacteria. Bright-field images of untreated bacteria were obtained as controls. For all experiments, suspensions of rhodamine isothiocyanate-modified AHAP/TEOS nanoparticles (500 μL of 10 or 50 μg mL^{-1} in PBS) were added to the bacteria on the glass slide. To observe association of NO-releasing particles with bacteria over time, fluorescence images were taken immediately following the addition of particles at 20 s intervals for 40 min. To compare the influence of particle size on the extent of particle−bacteria association, fluorescence images were obtained of bacteria treated with 10 μg mL^{-1} of 50, 100, and 200 nm particles for 10 min. After the 10 min incubation period, the suspension was removed, and the bacteria were copiously washed with fresh PBS to remove unassociated particles. Fresh PBS was then added, and the bacteria were imaged.

Cytotoxicity Assays. *In vitro* cellular toxicity of both control (*i.e.*, non-NO-releasing AHAP/TEOS particles) and NO-releasing particles of all three sizes was evaluated using L929 fibroblast cells. Briefly, the fibroblasts were cultivated in MEM supplemented with 10% fetal bovine serum (v/v) and 1% penicillin/streptomycin, then incubated in 5% CO_2/95% air under humidified conditions at 37 °C. After attaining confluency, the cells were trypsinized and then seeded onto tissue-culture-treated polystyrene 96-well plates at a density of 3×10^5 cells mL^{-1}. Three days later, cells were incubated with control and NO-releasing nanoparticles at a concentration range of 0−3.2 mg mL^{-1} for 2 h and 0−0.8 mg mL^{-1} for 24 h. Subsequently,

the particles were aspirated, cells were washed with sterile PBS three times, and 100 μL of fresh media was added to the cells. Cellular viability was assessed using the MTS assay (CellTiter 96 Aqueous Non-Radioactive Cell Proliferation Assay; Promega, Madison, WI). Briefly, the MTS reagent (20 μL) was added to each well until a purple formazan color was formed in the control (untreated) wells. The supernatant (90 μL) from each well was then transferred to a new 96-well plate prior to reading the absorbance at 490 nm using a microplate reader (Thermoscientific Multiskan EX; Waltham, MA). Untreated cells were used as controls, and results were expressed as percent viability relative to the untreated controls.

Acknowledgment. This work was supported by the National Institutes of Health (NIH EB000708) and Novan, Inc. A.W.C. also gratefully acknowledges a graduate research fellowship from Eastman Chemical Company (Kingsport, TN). The authors thank W. Storm for assistance in porosimetry measurements, Dr. M. ter Horst of the University of North Carolina at Chapel Hill for helpful discussions and technical assistance with ^{29}Si NMR, and Dr. N. Kramarcy at the Michael Hooker Microscopy Facility for support with confocal fluorescence microscopy.

Supporting Information Available: TEM images of 50, 100, and 200 nm nanoparticles, NO doses delivered from each particle concentration in cytotoxicity experiments, bacteria viability after exposure to control particles and blank (PBS), confocal images of time-based interaction between RITC-modified NO-releasing AHAP/TEOS particles and bacteria, confocal images of bacteria before and after treatment with RITC-modified NO-releasing AHAP/TEOS particles showing membrane disruption, cellular degradation, and blebbing. This material is available free of charge *via* the Internet at http://pubs.acs.org.

REFERENCES AND NOTES

1. Ignarro, L. J., *Nitric Oxide: Biology and Pathobiology*; Academic Press: San Diego, CA, 2000.
2. Bredt, D. S. Endogenous Nitric Oxide Synthesis: Biological Functions and Pathophysiology. *Free Radical Res.* **1999**, *31*, 577–597.
3. Hill, B. G.; Dranka, B. P.; Bailey, S. M.; Lancaster, J. R., Jr.; Darley-Usmar, V. M. What Part of NO Don't You Understand? Some Answers to the Cardinal Questions in Nitric Oxide Biology. *J. Biol. Chem.* **2010**, *285*, 19699–19704.
4. Zhang, J.; Snyder, S. H. Nitric Oxide in the Nervous System. *Annu. Rev. Pharmacol. Toxicol.* **1995**, *35*, 213–233.
5. Fang, F. C. Antimicrobial Reactive Oxygen and Nitrogen Species: Concepts and Controversies. *Nat. Rev. Microbiol.* **2004**, *2*, 820–832.
6. Ghaffari, A.; Miller, C. C.; McMullin, B.; Ghahary, A. Potential Application of Gaseous Nitric Oxide as a Topical Antimicrobial Agent. *Nitric Oxide* **2006**, *14*, 21–29.
7. Hrabie, J. A.; Keefer, L. K. Chemistry of the Nitric Oxide-Releasing Diazeniumdiolate ("Nitrosohydroxylamine") Functional Group and Its Oxygen-Substituted Derivatives. *Chem. Rev.* **2002**, *102*, 1135–1154.
8. Miller, M. R.; Megson, I. L. Recent Developments in Nitric Oxide Donor Drugs. *Br. J. Pharmacol.* **2007**, *151*, 305–321.
9. Seabra, A. B.; Duran, N. Nitric Oxide-Releasing Vehicles for Biomedical Applications. *J. Mater. Chem.* **2010**, *20*, 1624–1637.
10. Wang, P. G.; Cai, T. B.; Taniguchi, N. *Nitric Oxide Donors: For Pharmaceutical and Biological Applications*; Wiley-VCH: Weinheim, Germany, 2005.
11. Wang, P. G.; Xian, M.; Tang, X.; Wu, X.; Wen, Z.; Cai, T.; Janczuk, A. J. Nitric Oxide Donors: Chemical Activities and Biological Applications. *Chem. Rev.* **2002**, *102*, 1091–1134.
12. Scatena, R.; Bottoni, P.; Pontoglio, A.; Giardina, B. Pharmacological Modulation of Nitric Oxide Release: New Pharmacological Perspectives, Potential Benefits and Risks. *Curr. Med. Chem.* **2010**, *17*, 61–73.
13. Hetrick, E. M.; Shin, J. H.; Stasko, N. A.; Johnson, C. B.; Wespe, D. A.; Holmuhamedov, E.; Schoenfisch, M. H. Bactericidal Efficacy of Nitric Oxide-Releasing Silica Nanoparticles. *ACS Nano* **2008**, *2*, 235–246.
14. Shin, J. H.; Metzger, S. K.; Schoenfisch, M. H. Synthesis of Nitric Oxide-Releasing Silica Nanoparticles. *J. Am. Chem. Soc.* **2007**, *129*, 4612–4619.
15. Shin, J. H.; Schoenfisch, M. H. Inorganic/Organic Hybrid Silica Nanoparticles as a Nitric Oxide Delivery Scaffold. *Chem. Mater.* **2008**, *20*, 239–249.
16. Naizi, J. H.; Gu, M. B. *Toxicity of Metallic Nanoparticles in Microorganisms—a Review*; Springer: New York, 2009.
17. Morones, J. R.; Elechiguerra, J. L.; Camacho, A.; Holt, K.; Kouri, J. B.; Ramirez, J. T.; Yacaman, M. J. The Bactericidal Effect of Silver Nanoparticles. *Nanotechnology* **2005**, *16*, 2346–2353.
18. Kim, J. S.; Kuk, E.; Yu, K. N.; Kim, J. H.; Park, S. J.; Lee, H. J.; Kim, S. H.; Park, Y. K.; Park, Y. H.; Hwang, C. Y.; *et al*. Antimicrobial Effects of Silver Nanoparticles. *Nanomedicine* **2007**, *3*, 95–101.
19. Chen, X.; Schluesener, H. J. Nanosilver: A Nanoproduct in Medical Application. *Toxicol. Lett.* **2008**, *176*, 1–12.
20. Feng, Q. L.; Wu, J.; Chen, G. Q.; Cui, F. Z.; Kim, T. N.; Kim, J. O. A Mechanistic Study of the Antibacterial Effect of Silver Ions on *Escherichia Coli* and *Staphylococcus Aureus*. *J. Biomed. Mater. Res.* **2000**, *52*, 662–668.
21. Anyaogu, K. C.; Fedorov, A. V.; Neckers, D. C. Synthesis, Characterization, and Antifouling Potential of Functionalized Copper Nanoparticles. *Langmuir* **2008**, *24*, 4340–4346.
22. Esteban-Cubillo, A.; Pecharroman, C.; Aguilar, E.; Santaren, J.; Moya, J. S. Antibacterial Activity of Copper Monodispersed Nanoparticles into Sepiolite. *J. Mater. Sci.* **2006**, *41*, 5208–5212.
23. Mary, G.; Bajpai, S. K.; Chand, N. Copper (II) Ions and Copper Nanoparticles-Loaded Chemically Modified Cotton Cellulose Fibers with Fair Antibacterial Properties. *J. Appl. Polym. Sci.* **2009**, *113*, 757–766.
24. Adams, L. K.; Lyon, D. Y.; Alvarez, P. J. J. Comparative Eco-Toxicity of Nanoscale TiO_2, SiO_2, and ZnO Water Suspensions. *Water Res.* **2006**, *40*, 3527–3532.
25. Liu, Y.; He, L.; Mustapha, A.; Li, H.; Hu, Z. Q.; Lin, M. Antibacterial Activities of Zinc Oxide Nanoparticles against *Escherichia coli* O157:H7. *J. Appl. Microbiol.* **2009**, *107*, 1193–1201.
26. Rekha, K.; Nirmala, M.; Nair, M. G.; Anukaliani, A. Structural, Optical, Photocatalytic and Antibacterial Activity of Zinc Oxide and Manganese Doped Zinc Oxide Nanoparticles. *Physica B* **2010**, *405*, 3180–3185.
27. Zhang, L. L.; Jiang, Y. H.; Ding, Y. L.; Povey, M.; York, D. Investigation into the Antibacterial Behaviour of Suspensions of ZnO Nanoparticles (ZnO Nanofluids). *J. Nanopart. Res.* **2007**, *9*, 479–489.
28. Nair, S.; Sasidharan, A.; Rani, V. V. D.; Menon, D.; Nair, S.; Manzoor, K.; Raina, S. Role of Size Scale of ZnO Nanoparticles and Microparticles on Toxicity toward Bacteria and Osteoblast Cancer Cells. *J. Mater. Sci.: Mater. Med.* **2008**, *20*, 235–241.
29. Armelao, L.; Barreca, D.; Bottaro, G.; Gasparotto, A.; Maccato, C.; Maragno, C.; Tondello, E.; Stangar, U. L.; Bergant, M.; Mahne, D. Photocatalytic and Antibacterial Activity of TiO_2 and Au/TiO_2 Nanosystems. *Nanotechnology* **2007**, *18*, 375709–375716.
30. Brunet, L.; Lyon, D. Y.; Hotze, E. M.; Alvarez, P. J. J.; Wiesner, M. R. Comparative Photoactivity and Antibacterial Properties of C-60 Fullerenes and Titanium Dioxide Nanoparticles. *Environ. Sci. Technol.* **2009**, *43*, 4355–4360.
31. Choi, O.; Hu, Z. Q. Size Dependent and Reactive Oxygen Species Related Nanosilver Toxicity to Nitrifying Bacteria. *Environ. Sci. Technol.* **2008**, *42*, 4583–4588.
32. Martinez-Castanon, G. A.; Nino-Martinez, N.; Martinez-Gutierrez, F.; Martinez-Mendoza, J. R.; Ruiz, F. Synthesis and Antibacterial Activity of Silver Nanoparticles with Different Sizes. *J. Nanopart. Res.* **2008**, *10*, 1343–1348.
33. Lok, C. N.; Ho, C. M.; Chen, R.; He, Q. Y.; Yu, W. Y.; Sun, H.; Tam, P. K. H.; Chiu, J. F.; Che, C. M. Silver Nanoparticles: Partial Oxidation and Antibacterial Activities. *J. Biol. Inorg. Chem.* **2007**, *12*, 527–534.

34. Bagwe, R. P.; Yang, C.; Hilliard, L. R.; Tan, W. Optimization of Dye-Doped Silica Nanoparticles Prepared Using a Reverse Microemulsion Method. *Langmuir* **2004**, *20*, 8336–8342.
35. Arriagada, F. J.; Osseo-Asare, K. Synthesis of Nanosize Silica in a Nonionic Water-in-Oil Microemulsion: Effects of the Water/Surfactant Molar Ratio and Ammonia Concentrations. *J. Colloid Interface Sci.* **1999**, *211*, 210–220.
36. Chang, C.; Fogler, H. Controlled Formation of Silica Particles from Tetraethyl Orthosilicate in Nonionic Water-in-Oil Microemulsions. *Langmuir* **1997**, *13*, 3295–3307.
37. Jin, Y.; Lohstreter, S.; Pierce, D. T.; Parisien, J.; Wu, M.; Hall, C.; Zhao, J. X. Silica Nanoparticles with Continuously Tunable Sizes: Synthesis and Size Effects on Cellular Contrast Imaging. *Chem. Mater.* **2008**, *20*, 4411–4419.
38. Stjerndahl, M.; Andersson, M.; Hall, H. E.; Pajerowski, D. M.; Meisel, M. W.; Duran, R. S. Superparamagnetic Fe_3O_4/SiO_2 Nanocomposites: Enabling the Tuning of Both the Iron Oxide Load and the Size of the Nanoparticles. *Langmuir* **2008**, *24*, 3532–3536.
39. Han, Y.; Jiang, J.; Lee, S. S.; Ying, J. Y. Reverse Microemulsion-Mediated Synthesis of Silica-Coated Gold and Silver Nanoparticles. *Langmuir* **2008**, *24*, 5842–5848.
40. Yang, Y.; Jing, L.; Yu, X.; Yan, D.; Gao, M. Coating Aqueous Quantum Dots with Silica Via Reverse Microemulsion Method: Toward Size-Controllable and Robust Fluorescent Nanoparticles. *Chem. Mater.* **2007**, *19*, 4123–4128.
41. Yi, D. K.; Selvan, S. T.; Lee, S. S.; Papaefthymiou, G. C.; Kundaliya, D.; Ying, J. Y. Silica-Coated Nanocomposites of Magnetic Nanoparticles and Quantum Dots. *J. Am. Chem. Soc.* **2005**, *127*, 4990–4991.
42. Naka, Y.; Komori, Y.; Yoshitake, H. One-Pot Synthesis of Organo-Functionalized Monodisperse Silica Particles in W/O Microemulsion and the Effect of Functional Groups on Addition in Polystyrene. *Colloids Surf., A* **2010**, *361*, 162–168.
43. Bagwe, R. P.; Hilliard, L. R.; Tan, W. Surface Modification of Silica Nanoparticles to Reduce Aggregation and Nonspecific Binding. *Langmuir* **2006**, *22*, 4357–4362.
44. Brinker, C. J.; Scherer, G. W. *Sol-Gel Science: The Physics and Chemistry of Sol-Gel Processing*; Academic Press: San Diego, 1990.
45. Langevin, D. Micelles and Microemulsions. *Annu. Rev. Phys. Chem.* **1992**, *43*, 341–369.
46. Murdock, R. C.; Braydich-Stolle, L.; Schrand, A. M.; Schlager, J. J.; Hussain, S. M. Characterization of Nanomaterial Dispersion in Solution Prior to in Vitro Exposure Using Dynamic Light Scattering Technique. *Toxicol. Sci.* **2008**, *101*, 239–253.
47. Blosi, M.; Albonetti, S.; Dondi, M.; Martelli, C.; Baldi, G. Microwave-Assisted Polyol Synthesis of Cu Nanoparticles. *J. Nanopart. Res.* **2010**, *13*, 127–138.
48. Albert, K.; Bayer, E. Characterization of Bonded Phases by Solid-State NMR Spectroscopy. *J. Chromatogr.* **1991**, *544*, 345–370.
49. Hennel, J. W.; Klinowski, J. Magic-Angle Spinning: A Historical Perspective. *Top. Curr. Chem.* **2004**, *246*, 1–14.
50. Zhang, H.; Annich, G. M.; Miskulin, J.; Stankiewicz, K.; Osterholzer, K.; Merz, S. I.; Bartlett, R. H.; Meyerhoff, M. E. Nitric Oxide-Releasing Fumed Silica Particles: Synthesis, Characterization, and Biomedical Application. *J. Am. Chem. Soc.* **2003**, *125*, 5015–5024.
51. Clogston, J. D. *NCL Method PCC-2: Measuring Zeta Potential of Nanoparticles*; Nanotechnology Characterization Laboratory, N. C. I.: Frederick, MD, 2009.
52. Breed, R. S.; Dotterrer, W. D. The Number of Colonies Allowable on Satisfactory Agar Plates. *J. Bacteriol.* **1916**, *1*, 321–331.
53. Santra, S.; Yang, H.; Dutta, D.; Stanley, J. T.; Holloway, P. H.; Tan, W.; Moudgil, B. M.; Mericle, R. A. TAT Conjugated, FITC Doped Silica Nanoparticles for Bioimaging Applications. *Chem. Commun.* **2004**, *24*, 2810–2811.
54. Deupree, S. M.; Schoenfisch, M. H. Morphological Analysis of the Antimicrobial Action of Nitric Oxide on Gram-Negative Pathogens Using Atomic Force Microscopy. *Acta Biomater.* **2009**, *5*, 1405–1415.
55. Barbe, C.; Bartlett, J.; Linggen, K.; Finnie, K.; Qiang, L. H.; Larkin, M.; Calleja, S.; Bush, A.; Calleja, G. Silica Particles: A Novel Drug-Delivery System. *Adv. Mater.* **2004**, *16*, 1959–1966.
56. Thelestam, M.; Mollby, R. Cultured Human-Fibroblasts as a Model for Evaluation of Potential in Vivo Toxicity of Membrane Damaging Antibiotics. *Chem.-Biol. Interact.* **1980**, *29*, 315–325.
57. Lineaweaver, W.; McMorris, S.; Soucy, D.; Howard, R. Cellular and Bacterial Toxicities of Topical Antimicrobials. *Plast. Reconstr. Surg.* **1985**, *75*, 394–396.
58. Hetrick, E. M.; Schoenfisch, M. H. Analytical Chemistry of Nitric Oxide. *Ann. Rev. Anal. Chem.* **2009**, *2*, 409–433.
59. Riccio, D. A.; Nugent, J. L.; Schoenfisch, M. H. Stober Synthesis of Nitric Oxide-Releasing S-Nitrosothiol-Modified Silica Particles. *Chem. Mater.* **2010**, *23*, 1727–1735.